Andrea L. Nestor, George T. Cicila, Seth E. Karol, Kay M. Langenderfer, Stacy L. Hollopeter and David C. Allison
Physiol Genomics 25:286-293, 2006. First published Jan 24, 2006;
doi:10.1152/physiolgenomics.00135.2005

You might find this additional information useful...

Supplemental material for this article can be found at:
http://physiolgenomics.physiology.org/cgi/content/full/00135.2005/DC1

This article cites 56 articles, 20 of which you can access free at:
http://physiolgenomics.physiology.org/cgi/content/full/25/2/286#BIBL

Updated information and services including high-resolution figures, can be found at:
http://physiolgenomics.physiology.org/cgi/content/full/25/2/286

Additional material and information about ***Physiological Genomics*** can be found at:
http://www.the-aps.org/publications/pg

This information is current as of May 21, 2008 .

Physiological Genomics publishes results of a wide variety of studies from human and from informative model systems with techniques linking genes and pathways to physiology, from prokaryotes to eukaryotes. It is published quarterly in January, April, July, and October by the American Physiological Society, 9650 Rockville Pike, Bethesda MD 20814-3991. Copyright © 2005 by the American Physiological Society. ISSN: 1094-8341, ESSN: 1531-2267. Visit our website at http://www.the-aps.org/.

Downloaded from physiolgenomics.physiology.org on May 21, 2008

Physiol Genomics 25: 286–293, 2006.
First published January 24, 2006; doi: 10.1152/physiolgenomics.00135.2005.

Linkage analysis of neointimal hyperplasia and vascular wall transformation after balloon angioplasty

Andrea L. Nestor,[1,3] George T. Cicila,[2] Seth E. Karol,[1,3] Kay M. Langenderfer,[1,3] Stacy L. Hollopeter,[1,3] and David C. Allison[1,2,3]

Departments of [1]Surgery and [2]Physiology, Pharmacology, Metabolism, and Cardiovascular Science and [3]Medical University of Ohio Microscopy Imaging Center, Medical University of Ohio, Toledo, Ohio

Submitted 10 June 2005; accepted in final form 17 January 2006

Nestor, Andrea L., George T. Cicila, Seth E. Karol, Kay M. Langenderfer, Stacy L. Hollopeter, and David C. Allison. Linkage analysis of neointimal hyperplasia and vascular wall transformation after balloon angioplasty. *Physiol Genomics* 25: 286–293, 2006. First published January 24, 2006; doi: 10.1152/physiolgenomics.00135.2005.—Neointimal hyperplasia (NIH), a result of vascular injury, is due to the migration and proliferation of smooth muscle cells through the media and internal elastic lamina leading to vascular occlusion. We used a rat model to find the genetic regions controlling NIH after endothelial denudation in two divergent inbred strains of rats. The Brown Norway (BN) and spontaneously hypertensive rat (SHR) strains have a 2.5-fold difference in injury-induced NIH. A population of 301 F_2 (SHR × BN) rats underwent a standard vascular injury followed by phenotyping 8 wk after injury to identify quantitative trait loci (QTL) responsible for this strain difference. Interval mapping identified two %NIH QTL on rat chromosomes 3 and 6 [logarithm of odds (LOD) scores 2.5, 2.2] and QTL for other injured vascular wall changes on rat chromosomes 3, 4, and 15 (LOD scores 2.0–4.6). Also, QTL for control vessel media width (MW) and media area (MA) were found on chromosome 6 with LOD scores of 2.3 and 2.5, suggesting that linkage exists between these control vessel parameters and NIH production. These results represent the first genetic analysis for the identification of NIH QTL and QTL associated with the vascular injury response.

quantitative trait loci; restenosis; vascular injury; inbred strains; Brown Norway rat; spontaneously hypertensive rat

INTERVENTIONS IN THE CARDIOVASCULAR system such as arterial grafts, stents, and balloon angioplasties often fail because of the development of neointimal hyperplasia (NIH). There are no effective therapies to prevent or treat this complication. For example, restenosis secondary to NIH occurs in 30–40% of patients after balloon angioplasty for coronary artery disease (27). Drug-eluting stents reduce the occurrence of short-term NIH to 20–30%, but the long-term efficacy of these devices is not known (27). NIH is also associated with the development of significant restenosis in 20% of patients undergoing carotid endarterectomy (1) and is a major contributor to graft failure in coronary and peripheral arteries (24).

NIH is triggered by vascular endothelial cell (VEC) disruption and injury that leads to smooth muscle cell (SMC) migration to subendothelial injury sites, followed by SMC proliferation and apoptosis. Significant neointimal thickening and decreased lumen areas are seen within 2 wk after vascular injury (16, 32). However, vascular occlusion can continue after 2 wk as SMC size increases (16, 32) and proteoglycan matrix deposits continue to thicken the neointima (8, 28, 36, 37, 45). Many factors are involved in, and possibly responsible for, genetically determined variations in the NIH injury response between different strains of animals and among individual patients (1). We postulate that heritable variations in the genes for these vascular injury response elements are possible candidates for the quantitative trait loci (QTL) governing the differences in postinjury NIH among different individuals and animal strains.

We utilized a rat model for NIH formation after vascular injury to genetically dissect this complex biological process (1). In this model, we create a vascular injury by denuding the VECs of the vessel wall, similar to injury occurring in human vessels after cardiovascular interventions. The objective of the present work was to identify chromosomal regions containing the gene(s) responsible for the differences in NIH formation after vascular injury, previously observed between inbred spontaneously hypertensive rat (SHR) and Brown Norway (BN) rat strains (1). We performed a genome scan on a segregating population of 301 F_2 (SHR × BN) rats that identified multiple QTL for postinjury NIH and other vascular wall phenotypes.

MATERIALS AND METHODS

Animals. Inbred SHR and BN rats were obtained from Harlan Sprague-Dawley (Indianapolis, IN) and were maintained in the Division of Laboratory Animal Medicine at the Medical University of Ohio, where the genetic crosses were bred. Our previous experiments suggested that the alleles responsible for NIH growth were inherited in a codominant manner (1), and thus we selected an F_2 (SHR × BN) intercross population for the genome scan. Female SHR and male BN rats were intercrossed to produce F_1 (SHR × BN) progeny that were then used to breed an F_2 (SHR × BN) population of 301 males. Reciprocal crosses were not used to breed the initial F_1 population because of difficulties in BN rat husbandry. Therefore, the Y chromosome is inherited from the BN strain whereas the X chromosome is equally inherited from both strains. Male SHR and BN rats were also concomitantly raised for comparison. Rats were weaned at 28 days and fed a standard rat chow (Ralston Purina, Diet 5001) with ad libitum access to water.

Vascular injury. Surgery was performed on male rats at 11–12 wk of age (250–300 g) as previously described (1). Briefly, rats were anesthetized intraperitoneally with 80 mg/kg ketamine and 12 mg/kg xylazine, and the inner left thigh was shaved and disinfected. The skin over the femoral artery was opened, and the femoral artery was isolated by blunt dissection, dilated with lidocaine, and cannulated with a 2-Fr balloon catheter (1, 4). The 2-Fr balloon catheter was advanced to the distal aorta, inflated with 0.1 ml of normal saline, retracted, and deflated until slight resistance was encountered while

Article published online before print. See web site for date of publication (http://physiolgenomics.physiology.org).

Address for reprint requests and other correspondence: A. L. Nestor, Dept. of Surgery, Medical Univ. of Ohio, 3035 Arlington Ave., Toledo, OH 43614-5804 (e-mail: anestor@meduohio.edu).

1094-8341/06 $8.00 Copyright © 2006 the American Physiological Society

Downloaded from physiolgenomics.physiology.org on May 21, 2008

being withdrawn through the iliac artery. This process was repeated three times to ensure complete endothelial denudation. Finally, the left femoral artery was ligated, and the tissue layers and skin were approximated with an absorbable suture. This procedure produced the "standard vascular injury." This animal study was approved by the Medical University of Ohio Institutional Animal Care and Use Committee and complied with the *Guide for the Care and Use of Laboratory Animals* (National Institutes of Health Pub. No. 86-23, revised 1985).

Perfusion-fixation and preparation of vessel sections. Rats were anesthetized as above, and the body weight of each rat was recorded at the appropriate time intervals after surgery. A standard perfusion-fixation technique was performed as previously described (1). Primary agarose embedding was used before tissue processing and paraffin embedding to ensure an exact perpendicular orientation of the fixed vessels to the microtome blade. Each harvested vessel was "pinned out" on a straight axis in small, agarose-filled chambers. Once the agarose set, the embedded vessels were cut at the midpoint of the artery and submitted to standard paraffin processing. The "true" perpendicular axes of the midiliac arteries were then placed in blocks for sectioning. Midiliac artery sections were then stained with Verhoeff-van Gieson stain for elastin.

Vessel measurements. Image analysis measurements of the media area (MA), neointimal area (NIH area), and internal elastic lamina (IEL) length were made on perpendicular cross sections of control and injured arteries. These parameters were used to calculate the percentage of total arterial wall area due to neointimal growth (designated as %NIH), MA, media width (MW), circular area (CA), and lumen size (LS) of each vessel (1). Body weight-adjusted heart weight (BWadj-HW) was calculated by adjusting heart weight for differences in body weight, using the regression of heart weight on body weight for each animal (14, 21). Because lumens of sectioned vessels were sometimes partially collapsed, the CA was calculated with the length of the IEL directly measured by image analysis. CAs were calculated by the formula $CA = (IEL)^2/4\pi$. To correct for asymmetric neointimal growth in the injured vessels, injured vessel lumen size (inj-LS) was calculated by subtracting the neointimal area of each vessel from its CA: inj-LS = CA − neointimal area. As control vessels did not have a neointimal layer, their CA and LS were identical. The MA of each vessel was directly measured and, in conjunction with IEL length, allowed calculation of MW as follows:

$$MW = r_2 - r_1 \quad (1)$$

where r_2 is the radius of the entire vessel and r_1 is the radius of its CA.

$$\text{area of entire vessel} = \pi(r_2)^2$$

$$= CA + MA \text{ or, substituting, } \frac{IEL^2}{4\pi} + MA \quad (2)$$

Therefore,

$$r_2 = \sqrt{\frac{\frac{IEL^2}{4\pi} + MA}{\pi}} \quad (3)$$

Because $r_1 = IEL/2\pi$,

$$MW = \sqrt{\frac{\frac{IEL^2}{4\pi} + MA}{\pi}} - \frac{IEL}{2\pi} \quad (4)$$

In addition to BWadj-HW, 10 vascular parameters were measured: parameters related to vascular injury include injured vessel CA, injured vessel MA, injured vessel MW, injured vessel NIH area, injured vessel MA + NIH area, injured vessel LS, and injured vessel %NIH. We also measured parameters in the control vessels that were not related to the vascular injury, including control vessel CA, control vessel MA, and control vessel MW.

Statistical analysis. Distributions of each phenotype in the F_2 (SHR × BN) population were assessed for normality with the SPSS computer program (SPSS, Chicago, IL) by skewness, kurtosis, and the Kolmogorov-Smirnov test. Of the phenotypes measured, two required transformation for normality as follows: %NIH values were transformed by taking the square root and BWadj-HW values were normalized by removing outliers from Box Plot analysis and then taking 1 divided by the value ($1/X$). Both of the transformed phenotypic values (%NIH and BWadj-HW) were found to have a normal distribution by the Kolmogorov-Smirnov test. Many of the distributions were nearly (98.8%) normal and only required removal of outliers as determined by Box Plot analysis. Furthermore, statistical analyses of differences and/or associations between these parameters measured in the parental and F_2 (SHR × BN) rats were also analyzed with one-way ANOVA, χ^2 and a nonparametric statistical method to test for possible associations between these parameters without assumptions about their underlying distribution.

Genotyping with PCR. Microsatellite loci were genotyped by PCR amplification. Genomic DNA was prepared from the unfixed livers of BN, SHR, and F_2 (SHR × BN) rats isolated with a kit (Dneasy 96-well kit, Qiagen, Valencia, CA). PCR amplification was performed with a PTC-100-96Ag thermocycler (MJ Research, Waltham, MA) as previously described (53). PCR products were electrophoretically size-fractionated on 4% 3:1 (Amresco, Solon, OH) or 4% Metaphor (Cambrex Bio Science, Walkersville, MD) agarose gels and visualized with ethidium bromide staining.

Identification of putative QTL by interval mapping. Putative QTL were first identified by selective genotyping of a portion of the F_2 (SHR × BN) population. Specifically, the highest ($n = 45$) and lowest ($n = 45$) 15% of the population with regard to NIH formation were genotyped with polymorphic microsatellite markers, spaced on average 13–25 cM apart (see Supplemental Table S1, which is available at the *Physiological Genomics* web site).[1] The Map Manager QTX computer program (35) was used to order genotypic data into linkage groups, perform interval mapping, and identify putative QTL (29, 44). Potential errors in typing, i.e., loci involved in double-recombination events, were retyped to confirm or correct the results. Threshold values for suggestive linkage of a locus to a QTL were as defined by Lander and coworkers (29, 30), corresponding to the expectation of one false positive per genome scan. Each rat chromosome (RNO) that contained at least one marker suggesting linkage in this %NIH-directed genome scan (RNO2–RNO7, RNO15, and RNO20) was genotyped for the remaining 211 F_2 (SHR × BN) rats in the population. Additional microsatellite markers were genotyped in chromosomal regions identified as containing putative QTL in the first phase of the genome scan. Map Manager QTX (35) was used to organize interval maps of the chromosomal regions containing NIH QTL.

RESULTS

Genome scan. %NIH was measured in the injured vessels of 301 F_2 (SHR × BN) rats 8 wk after a standard vascular injury. Initially, 158 markers were used to selectively genotype microsatellite polymorphisms covering rat chromosomes (1–20, X) in the F_2 (SHR × BN) population, with the highest (top 15%, $n = 45$) and lowest (bottom 15%, $n = 45$) %NIH selected from 301 male F_2 rats after the standard vascular injury. Chromosomal regions with logarithm of odds (LOD) scores suggestive of linkage (≥2.0) to the measured phenotype for both control and injured vessel phenotypes, %NIH, MA, NIH

[1] The Supplemental Material for this article (Supplemental Table S1) is available online at **http://physiolgenomics.physiology.org/cgi/content/full/00135.2005/DC1**.

Downloaded from physiolgenomics.physiology.org on May 21, 2008

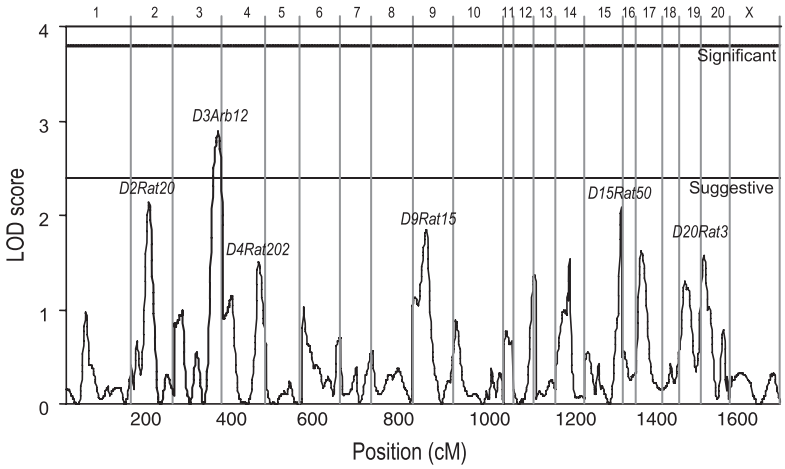

Fig. 1. Logarithm of odds (LOD) plot of the %NIH genome scan quantitative trait loci (QTL) identified with a free mode of inheritance. Results are from the selective portion of the F_2 [spontaneously hypertensive (SHR) × Brown Norway (BN)] population (n = 90) of postinjury %NIH analyzed with 158 polymorphic microsatellite markers.

area, MA + NIH area, CA, LS, MW, and BWadj-HW, were then selected for genotyping in the remaining 211 rats of the F_2 (SHR × BN) population. The average spacing of microsatellite markers was 13.6 cM, with a mean maximum distance of 25.1 cM between markers on a chromosome, resulting in 99.4% of the genome being within 15 cM of a microsatellite marker (see Supplemental Table S1). The resulting map length using the Kosambi correction of all rat chromosomes was 1,780.3 cM, similar to previous estimates (5, 7, 15).

Figure 1 shows a LOD plot of the F_2 (SHR × BN) genome scan for the %NIH phenotype based on the top and bottom 15% of postinjury NIH formation (n = 90 rats). This LOD plot for the %NIH genome scan used a free model of inheritance without any assumptions regarding inheritance. Three chromosomal regions showed suggestive linkage to %NIH in this initial screen: *1*) RNO2, with a peak LOD score near *D2Rat20*; *2*) RNO3, with a peak LOD score near *D3Arb12*; and *3*) RNO15, with a peak LOD score near *D15Rat50* (Fig. 1). QTL for vascular wall measurements of control and injured vessels, as well as for BWadj-HW (RNO2, near marker *D2Rat111*) were also found in this initial, %NIH-directed genome scan; these include QTL for control vessel measurements unrelated to NIH formation for MA, CA, LS, and MW on RNO2 near marker *D2Rat3*, MA, CA, and LS on RNO4 near marker *D4Rat198*, and MA and MW on RNO6 near marker *D6Rat44*. Furthermore, vascular wall measurements of injured vessel QTL related to NIH growth were found for MA on RNO4 near marker *D4Rat198*, CA and LS on RNO5 near marker *D5Rat20*, as well as MA on RNO7 and RNO20 near markers *D7Rat20* and *D20Rat1*, respectively. Complete genotyping of these QTL by chromosome was then performed for the remaining 211 F_2 (SHR × BN) rats for RNO2–RNO7, RNO15, and RNO20.

Table 1 summarizes the characteristics of the QTL confirmed in the complete F_2 (SHR × BN) population of 301 rats, including the locus nearest the LOD plot peak for each phenotype and its mean value for the three genotypes. The mode of inheritance resulting in the highest significant LOD score for each QTL is also given (30). Fourteen QTL were found, of which only ten (injured vessel QTL) were directly related to postinjury NIH production (Table 1). LOD plots for the QTL identified on RNO3, RNO4, RNO6, and RNO15 are shown in Fig. 2, *A–D*, respectively. Two significant QTL for injured vessel CA (LOD 4.6) and inj-LS (LOD 4.2) were found on RNO3 located near marker *D3Arb12* (Fig. 2*A*). We also found

Table 1. *QTL identified with Map Manager QTX in F_2 (SHR × BN) population for %NIH*

RNO	Parameter	Vessel	Locus	Genotype			LOD	Model
				BN/BN	BN/SHR	SHR/SHR		
3	MA, mm^2	Injured	*D3Rat227*	0.092±0.02	0.095±0.02	0.103±0.02	2.0	Dominant
3	CA, mm^2	Injured	*D3Rat12*	0.416±0.08	0.436±0.08	0.471±0.11	2.9	Free
3	LS, mm^2	Injured	*D3Rat12*	0.392±0.08	0.415±0.08	0.450±0.10	2.8	Free
3	CA, mm^2	Injured	*D3Arb12*	0.409±0.07	0.448±0.11	0.456±0.09	4.6	Free
3	%NIH	Injured	*D3Arb12*	0.182±0.12	0.188±0.13	0.125±0.09	2.5	Dominant
3	LS, mm^2	Injured	*D3Arb12*	0.387±0.07	0.431±0.09	0.432±0.11	4.2	Free
3	NIH area, mm^2	Injured	*D3Arb12*	0.023±0.02	0.025±0.02	0.016±0.01	3.1	Dominant
4	MA + NIH area, mm^2	Injured	*D4Rat79*	0.119±0.03	0.114±0.03	0.128±0.03	2.3	Dominant
6	%NIH	Injured	*D6Rat44*	0.198±0.13	0.157±0.11	0.169±0.12	2.2	Recessive
6	MA, mm^2	Control	*D6Rat44*	0.106±0.02	0.098±0.02	0.096±0.02	2.5	Recessive
6	MW, mm^2	Control	*D6Rat44*	0.042±0.01	0.040±0.01	0.047±0.06	2.3	Recessive
6	MA, mm^2	Control	*D6Rat150*	0.105±0.02	0.096±0.02	0.098±0.02	2.5	Recessive
6	MW, mm^2	Control	*D6Rat150*	0.042±0.01	0.040±0.01	0.044±0.03	2.3	Recessive
15	MA, mm^2	Injured	*D15Rat95*	0.093±0.02	0.095±0.02	0.104±0.03	2.4	Dominant

Data are means ± SD; all 301 F_2 [spontaneously hypertensive rat (SHR) × Brown Norway (BN)] animals were genotyped in quantitative trait loci (QTL) regions. RNO, rat chromosome; MA, media area; CA, circular area; LS, lumen size; NIH, neointimal hyperplasia; %NIH, % of total arterial wall area due to neointimal growth; MW, media width; Locus, locus nearest QTL peak; LOD, logarithm of odds ratio; Model, mode of inheritance resulting in LOD score with highest significance.

Downloaded from physiolgenomics.physiology.org on May 21, 2008

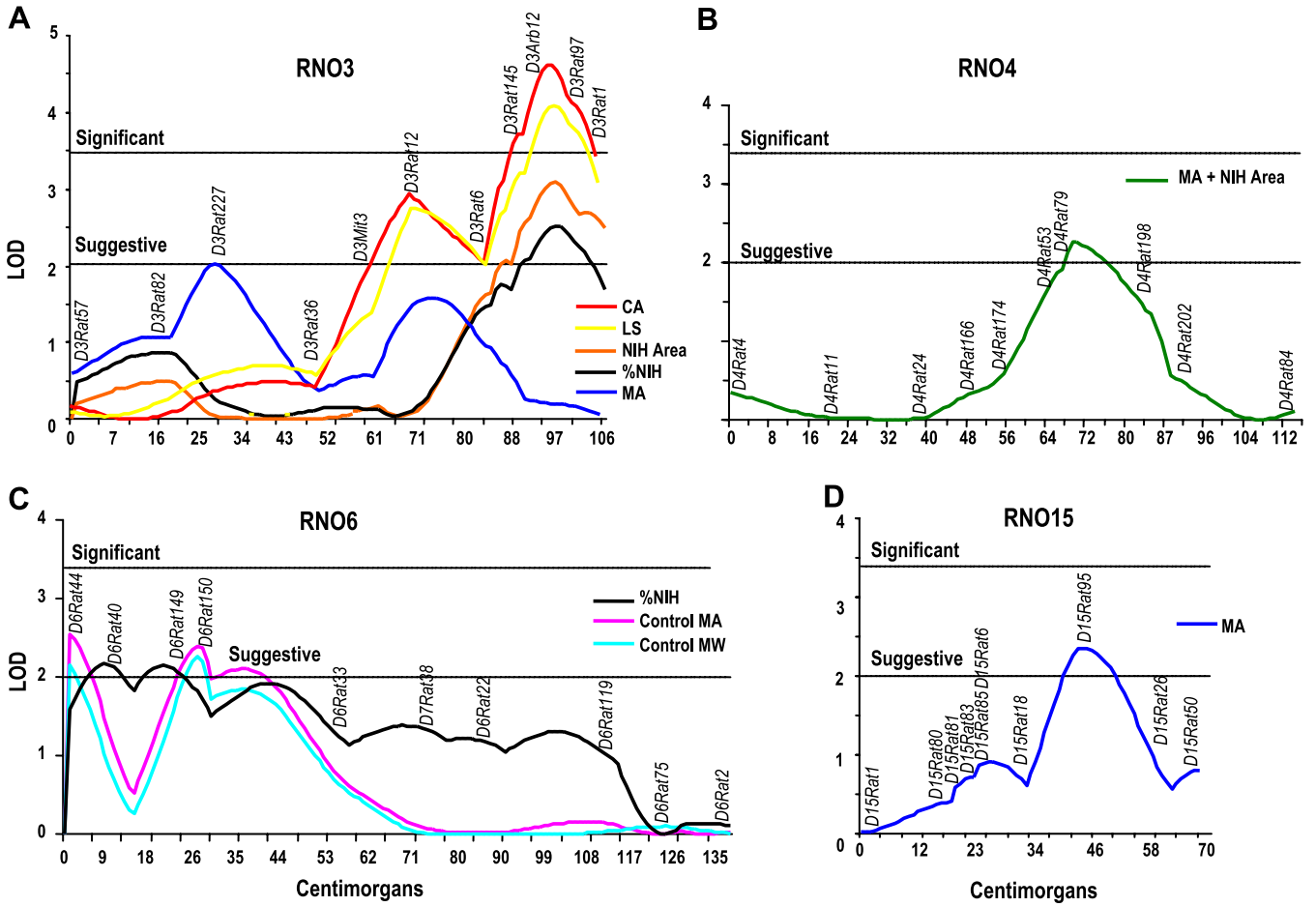

Fig. 2. Individual LOD plots for phenotypes measured in the %NIH-driven genome scan. Linkage for postinjury NIH production and other vessel-wall phenotypes were found on rat chromosomes RNO3 (*A*), RNO4 (*B*), RNO6 (*C*), and RNO15 (*D*) for the F_2 (SHR × BN) population ($n = 301$). Thresholds differ for the individual chromosomes because of the use of different models of inheritance (30). CA, circular area; LS. lumen size; NIH, neointimal hyperplasia; MA, media area; MW, media width.

several suggestive QTL related to injured vessel MA, CA, LS, NIH area, and %NIH, primarily residing in the same area of the distal portion of the q arm of RNO3 (Fig. 2*A*). The RNO3 QTL associated with injured vessel MA (blue) was located near *D3Rat227*, with a LOD score of 2.0. The RNO3 QTL associated with injured vessel CA (red) were located near *D3Rat12 and D3Arb12*, with LOD scores of 2.9 and 4.6. Also in the q terminus of RNO3 located near *D3Arb12* are QTL for %NIH, injured vessel LS, and NIH area. The %NIH (transformed data, black) and NIH area (nontransformed data, orange) QTL have similar LOD plots peaking near *D3Arb12* and LOD scores of 2.5 and 3.1, respectively. Finally, QTL peaks were found near both *D3Rat12* (LOD = 2.8) and *D3Arb12* (LOD = 4.2) for injured vessel LS (yellow).

Suggestive QTL were also identified on RNO4, RNO6, and RNO15 (Fig. 2, *B–D*, respectively): a QTL for MA + NIH area was found on RNO4, with a peak LOD score of 2.3 near *D4Rat79* (Fig. 2*B*). RNO6 had two suggestive %NIH QTL peaks near *D6Rat40* and *D6Rat149*, respectively, both with LOD scores of 2.2 (Fig. 2*C*). RNO6 also had QTL for two control vessel measurements, MA and MW, at the distinct *D6Rat44* and *D6Rat150* loci. The control vessel MA and MW QTL had similar LOD plots with LOD scores of 2.5 and 2.3, respectively (Fig. 2*C*). An injured vessel MA QTL was found on RNO15 with a LOD score of 2.4 located near *D15Rat95* (Fig. 2*D*).

BWadj-HW and control vessels. Table 2 shows the mean ± %CV of BWadj-HW and the CA, MA, and MW of BN, SHR, and F_2 (SHR × BN) control vessels harvested 8 wk after the vascular injury. The mean BWadj-HW of the hypertensive SHR rats was significantly higher than that of normotensive BN rats (Table 2), with the mean BWadj-HW F_2 (SHR × BN) values intermediate to those of the parental strains ($P < 0.001$, Table 2). Also, SHR control vessels had smaller CA and larger MA and MW than BN control vessels (Table 2). No associations were found between BWadj-HW and control vessel CA of the individual BN and F_2 (SHR × BN) rats [P = not significant (NS)]. Furthermore, the F_2 (SHR × BN) control vessels had larger CA than SHR control vessels ($P < 0.001$, Table 2).

Injured and control vessels. In a preliminary time after injury study, BN and SHR vessels were harvested at 0, 2, 4, 7, 18, 23, and 28 days in addition to 8 wk after injury. There was considerable scatter in the measurements of the vessels taken at these earlier time periods. The only significant difference found was a relative increase in the BN vessel NIH area and %NIH at 8 wk after injury ($P < 0.05$; data not shown). However, injury-induced neointima was observed in both

Downloaded from physiolgenomics.physiology.org on May 21, 2008

Table 2. *Vascular parameters measured for control BN, SHR, and F_2 (SHR × BN) vessels*

Parameter	BN	SHR	F_2 (SHR × BN)
CA, mm^2	0.454±46 (0.285–1.171)	0.342±13 (0.247–0.414)*	0.439±25 (0.214–1.149)
MA, mm^2	0.087±25 (0.056–0.136)	0.094±22 (0.061–0.131)	0.100±21 (0.056–0.197)
MW, mm^2	0.035±13 (0.027–0.043)*	0.042±18 (0.027–0.057)	0.040±16 (0.025–0.067)‡
BWadj-HW, g	1.104±34 (0.953–1.298)*† (n=12)	1.559±7 (1.384–1.804)‡ (n=18)	1.439±14 (1.064–2.879)‡ (n=279)

Data are means ± %CV, with range given in parenthesis, for 16 BN, 20 SHR, and 301 F_2 (SHR × BN) control vessels. Control and contralateral injured vessels were harvested 8 wk after standard vascular injury. Body weight-adjusted heart weight (BWadj-HW) was calculated by adjusting heart weight for differences in body weight, using regression of heart weight on body weight. *$P < 0.001$ vs. F_2 (SHR × BN) by 1-way ANOVA; †$P < 0.001$ vs. SHR by 1-way ANOVA; ‡$P < 0.001$ vs. BN by 1-way ANOVA.

strains only 2 days after the vascular injury, arguing against differences in intimal denudations from the initial injury being responsible for the 8-wk strain differences in neointima production. The IEL in sections of these vessels from the early postinjury time points were also graded in a coded study for the "number of IEL breaks" and "waviness or corrugation" (graded 0–6), a morphology pattern associated with reactive vasospasm (3, 16, 33). Interestingly, the sections of the vessels taken 0–18 days after injury (30 vessels from each strain) revealed that the SHR IEL had more breaks (mean = 14.3, range 2 to >40) than the BN IEL (mean = 8.7, range 0–32, $P < 0.025$). Surprisingly, the average "wave grade" of the injured BN vessels was 2 (range 0–6), compared with only 0.6 (range 0–3) for the injured SHR vessels ($P < 0.001$). Together, these results are consistent with the thinner BN vessels (see below, Tables 2 and 3), which are also more fragile than the SHR vessels (11, 23), being more easily distended than the more rigid SHR vessels. Thus the BN vessels had fewer injury-induced IEL breaks. This difference in injury pattern between the two strains, i.e., the numbers of injury-induced IEL breaks, may have led to differences in injury-induced vasospasm (waves) and possibly contributed to the strain variations in neointimal growth.

Injured BN vessels did have higher NIH area and %NIH than injured SHR vessels (Table 3; Ref. 1). In contrast to our earlier results (1), this increased neointima formation was not associated with a smaller LS for the injured BN vessels, which had a 10% increase in CA compared with the noninjured control vessels, compensating for the occlusive effects of the NIH ingrowth (Table 4). However, the NIH ingrowth in the injured F_2 (SHR × BN) vessels did lead to a significant decrease in LS compared with control vessels (Table 4).

The F_2 (SHR × BN) control vessels were similar to the BN control vessels and showed strong associations between individual vessel CA and MA ($P < 0.001$) but also resembled the SHR control vessels, with strong associations found between individual MW and MA ($P < 0.001$). In summary, the control vessels of BN and SHR rats showed strain-specific associations of the CA, MA, and MW, with the control vessels of the F_2 (BN × SHR) rats having attributes of both parental strains. Most importantly, for both of the parental BN and SHR rat strains, no associations were found between the individual control vessel CA, MA, MW, and BWadj-HW measurements and any of the parameters measured in the injured vessels of the same rats (P = NS). In contrast, control vessel MW of individual F_2 (SHR × BN) rats were significantly related to the injured vessel MA ($P < 0.001$) and MW ($P < 0.001$) of the same F_2 rats. Furthermore, values of the individual F_2 (SHR × BN) injured vessel MA, MW, CA, MA + NIH area, and %NIH were all positively associated ($P < 0.001$). Finally, the BWadj-HW of individual F_2 (SHR × BN) rats also showed a positive association with the injured vessel CA, MA + NIH area, and %NIH ($P < 0.001$).

DISCUSSION

Ultimately, we would like to facilitate the discovery of effective therapies to prevent vascular restenosis by taking advantage of the 2.5-fold difference in NIH formation found between the inbred BN and SHR rat strains (1). The genome scan of the F_2 (SHR × BN) intercross population identified regions controlling the formation of NIH on RNO3 and RNO6. Surprisingly, the %NIH-directed genome scan led to the discovery of QTL for vascular wall parameters in both control and injured vessels that were not directly related to NIH formation. The injured vessel vasculature changes were associated with QTL for MA, CA, and LS on RNO3 (Fig. 2*A*), MA + NIH area on RNO4 (Fig. 2*B*), and MA on RNO15 (Fig. 2*D*). The control vessel vasculature changes were particularly interesting, with QTL for both MA and MW found in two distinct peaks on RNO6 (Fig. 2*C*).

Table 3. *Vascular parameters measured for injured BN, SHR, and F_2 (SHR × BN) vessels*

Parameter	BN	SHR	F_2 (SHR × BN)
CA, mm^2	0.500±70 (0.290–1.790)	0.347±22 (0.273–0.591)*	0.442±21 (0.092–0.858)†
LS, mm^2	0.471±73 (0.261–1.742)	0.335±24 (0.217–0.580)*	0.420±21 (0.091–0.846)†
MA, mm^2	0.072±37 (0.039–0.148)*	0.088±26 (0.046–0.126)	0.097±23 (0.029–0.174)‡
MW, mm^2	0.028±20 (0.020–0.040)*†	0.040±21 (0.024–0.053)‡	0.039±18 (0.021–0.062)‡
NIH area, mm^2	0.029±58 (0.005–0.058)	0.012±118 (0.001–0.058)	0.022±85 (0.000–0.104)
MA + NIH area, mm^2	0.101±37 (0.048–0.197)	0.100±25 (0.062–0.148)	0.118±25 (0.030–0.224)
%NIH	0.271±41 (0.070–0.442)*†	0.116±97 (0.004–0.391)	0.171±70 (0.001–0.613)‡

Data are means ± %CV, with range given in parenthesis, for 16 BN, 20 SHR, and 301 F_2 (SHR × BN) vessels harvested 8 wk after the standard vascular injury. *$P < 0.001$ vs. F_2 (SHR × BN) by 1-way ANOVA; †$P < 0.001$ vs. SHR by 1-way ANOVA; ‡$P < 0.001$ vs. BN by 1-way ANOVA.

Downloaded from physiolgenomics.physiology.org on May 21, 2008

Table 4. *Comparison of parameters measured for control and injured BN, SHR, and F_2 (SHR × BN) vessels*

Parameter	*n*	CA, mm²	MA, mm²	MW, mm²	MA + NIH area, mm²	LS, mm²
BN control	16	0.454±46	0.087±25	0.035±13	0.087±25	0.454±46
BN injured	16	0.500±70	0.072±37	0.028±20	0.101±37	0.471±73
P, 1-way ANOVA		NS	NS	0.001	NS	NS
SHR control	20	0.342±13	0.094±22	0.042±18	0.094±22	0.342±13
SHR injured	20	0.347±22	0.088±26	0.040±21	0.100±25	0.335±24
P, 1-way ANOVA		NS	NS	NS	NS	NS
F_2 control	301	0.439±25	0.100±21	0.040±16	0.100±21	0.439±25
F_2 injured	301	0.442±21	0.097±23	0.039±18	0.118±25	0.420±21
P, 1-way ANOVA		NS	NS	0.002	<0.0001	0.019

Data are means ± %CV. NS, not significant.

Several NIH-related and injured vessel QTL were found on the distal arm of RNO3 (Fig. 2*A*): a QTL-containing region was identified on RNO3 near marker *D3Arb12* for %NIH, NIH area, CA, and LS. In addition, QTL were found on RNO3 for injured vessel MA near marker *D3Rat227* as well as LS and CA near marker *D3Rat12*. We have examined these regions of the rat genome for known genes and are targeting several candidates for further study that may be controlling the NIH injury response.

Initially, vascular injury triggers platelet aggregation and release of *PDGF* (1, 39), a chemoattractant for SMCs in the media and other inflammatory cells in the circulation and adjacent tissues (39). SMCs migrate through the ECM of the media, pass through the injured IEL, and proliferate and undergo apoptosis at the subendothelial injury site. SMC migration and proliferation are both triggered and modulated by *PDGF* (32, 48, 54), *TGFβ* (32, 36, 40, 48), endothelial cell-produced heparin (32, 45), estradiol (19), progesterone (31), *IGF-I* and *IGF-II* (48), *EGF* (48), basic fibroblastic growth factor (*bFGF*) (48), somatomedin C (32), epidermal growth factor (48), *IL-1* (48), and enzymes, some possibly related to the renin-angiotensin-aldosterone system (13, 45). ECM macromolecules such as collagen, elastin, proteoglycans, and adhesive glycoproteins are also involved in maintaining vascular wall integrity after injury (17, 28, 36, 37), and signaling cascades induced by changes in these ECM macromolecules can regulate the migration (6, 45, 51), apoptosis (6, 18, 41), proliferation (16, 32, 45), and differentiation (34) of vascular SMCs, VECs, and fibroblasts. Intriguingly, the QTL interval on RNO3 includes matrix metalloproteinase-9 (*Mmp9*) and cadherin 22 (*Cdh22*).

The MMP family consists of 17 known enzymes classified as collagenases, gelatinases, stromelysins, and metalloelastases. *Mmp9*, of the gelatinase subfamily, is located within the NIH QTL region on RNO3 near locus *D3Arb12* and is involved in remodeling the vascular ECM (20). MMP enzymatic activation is controlled by inducible nitric oxide synthase (iNOS) signaling. The endothelial nitric oxide synthase (eNOS) isoforms are constitutively active and produce NO in small quantities. eNOS protects the uninjured vasculature by inducing vasorelaxation in response to the shear stress of increased blood pressure (2, 10, 42), inhibits the transvascular migration and proliferation of SMCs and leukocytes (2, 9, 12, 52), blocks the adherence and aggregation of platelets to the vessel walls (2, 9, 12, 38, 52), and promotes endothelial cell growth and proliferation (2). iNOS produces NO in large quantities, is stimulated by vascular damage, and abrogates the vascular protective effects of eNOS-produced NO. NO produced by iNOS thereby promotes injury-induced vasospasm, adherence and aggregation of platelets to the injury site, transvessel migration of SMCs and inflammatory cells (2, 9, 12, 26, 38, 52), and upregulation of MMP expression (26). MMP expression leads to the enzymatic degradation of the ECM and facilitates SMC migration through the media and IEL of the injured vessel.

Another candidate gene in the RNO3 QTL-containing region is a cadherin, *Cdh22*. Cadherins are adhesion molecules involved in calcium-dependent cell-cell adhesions and may aid the migration of SMCs through the ECM. *Cdh22* also participates in a signal transduction pathway regulating expression levels and localization of β-catenin, which also controls cell proliferation, migration, and apoptosis by the *Wnt* growth factor pathway (22). We also scanned genes present in the RNO6 QTL-containing region. Although several genes could potentially be involved in the process of NIH formation, none was as obvious a candidate as *Mmp9* and *Cdh22* for governing the NIH injury response.

We previously found (1) slight decreases in the CA (P = NS) and LS of injured BN vessels compared with noninjured controls. It was possible, however, that this finding was in part due to the noninjured BN vessels being more flexible and difficult to properly orient in the tissue blocks for perpendicular sections than the injured vessels, i.e., the noninjured vessels lacked the rigidity of the injured vessels imparted by the neointima itself and the postinjury inflammatory response. If this was the case, such bias in section perpendicularity would artificially elevate the control vessel CA values. In the present study, we used primary agarose embedding before processing and paraffin embedding to ensure an exact perpendicular orientation of the fixed vessels to the microtome blade (see MATERIALS AND METHODS). A different result from that previously was found for sections prepared in this manner, with a 10% increase of CA of the injured BN vessels occurring, which more than compensated for any occlusive effects of the neointima on the LS of the injured BN vessels (P = NS, Table 1).

BWadj-HW and vessel-wall parameters such as CA, MW, and %NIH are complex phenotypes, presumably controlled by the interplay of multiple genetic and environmental factors. Phenotypes influenced by the same environmental or genetic factors are expected to have expression levels that are positively or negatively linked. Phenotypes without common underlying causal factors would not be expected to show a coordinated pattern of expression. Also, the degree of expression of certain phenotypes before injury might influence the

Downloaded from physiolgenomics.physiology.org on May 21, 2008

extent, and thereby the subsequent repair, of the standard vascular injury, i.e., the standard vascular injury might produce different degrees of damage to thick- and thin-walled vessels. If this were the case, then the initial MA or MW of a given F_2 (SHR × BN) vessel might have a direct bearing on the amount of injury transmitted to that vessel and, in turn, influence its postinjury NIH production. In support of this, the differing numbers of postinjury IEL "breaks" and "waves" between the BN and SHR parental strains also suggest that a genetic difference in vessel fragility and distensibility (11, 23) may directly influence the postinjury responses of the vasculature. We are currently trying to determine whether or not these differences in postinjury vascular changes between the BN and SHR strains can be influenced by endothelial vasodilators.

As the SHR rat is perhaps the best-studied genetic model of hypertension and F_2 (SHR × BN) populations are extensively used to identify QTL for blood pressure and related traits (46, 49, 50), elevated blood pressures may have influenced the response to the standard vessel injury in our population of F_2 (SHR × BN) rats. Each of the F_2 (SHR × BN) rats in our population was phenotyped for BWadj-HW, which shows a strong correlation with blood pressure in rat models (43, 55), including segregating populations of rats (reviewed in Ref. 47). Here we used BWadj-HW as an indirect (and imperfect) measure of the blood pressures observed in the population. As expected, the mean BWadj-HW of F_2 (SHR × BN) rats was intermediate to, and significantly different from, the higher values of SHR rats and the lower values of BN rats (Table 2). The lack of association between BWadj-HW and control vessel CA of the individual BN and F_2 (SHR × BN) rats and the increased CA observed in F_2 (SHR × BN) control vessels, compared with those of SHR control vessels (Table 2), suggest that the mechanism(s) producing small, thick-walled vessels in the SHR rats is not present in the F_2 (SHR × BN) rats.

The finding of QTL for non-NIH-related phenotypes, especially those for control vessel MA and MW (Table 1), in the %NIH-driven genome scan supports the possibility of causal connections between certain control vessel parameters and postinjury NIH production. Specifically, the initial genome scan was performed on rats at the extremes of the F_2 (SHR × BN) %NIH phenotypic distribution, followed by genotyping of the remaining F_2 rats in the chromosome regions where QTL were identified. The complete %NIH-driven genome scan revealed 14 QTL, of which only 10 (injured vessel parameters) were directly related to NIH (Table 1). The non-NIH-related QTL (control vessel parameters) can only be explained by chance or causal connections between postinjury NIH and these phenotypes.

If future studies with congenic strains confirm these associations between the control vessel parameters and postinjury neointima production, these relationships may allow the identification of vessels or individuals with an increased susceptibility to NIH after vascular procedures. Also, development of congenic strains that delimit the chromosomal intervals in which causative gene(s) for %NIH-related QTL reside should facilitate the future identification of the genes responsible for the strain differences in postinjury NIH formation observed between BN and SHR rats. This discovery may, in turn, facilitate the identification of orthologous, NIH-related genes in humans, as disease-specific QTL found in rodent studies have often been shown to be located within orthologous human chromosomal regions containing QTL for the same (or related) phenotypes (25, 56). Ultimately, the detection of NIH QTL may lead to the identification of the gene(s) controlling vascular stenosis and the development of new therapies to prevent this complication.

ACKNOWLEDGMENTS

We thank Dawn Pauli for technical assistance with genotyping and maintenance of the rat colony.

GRANTS

This research was supported by American Heart Association Ohio Valley Affiliate Grant 0051562B to D. C. Allison and National Heart, Lung, and Blood Institute Grant HL-68994 to G. T. Cicila, as well as the Cancer Biology Fund of the Medical University of Ohio Foundation.

REFERENCES

1. **Assadnia S, Rapp JP, Nestor AL, Pringle T, Cerilli GJ, Gunning WT 3rd, Webb TH, Kligman M, and Allison DC.** Strain differences in neointimal hyperplasia in the rat. *Circ Res* 84: 1252–1257, 1999.
2. **Barbato JE and Tzeng E.** Nitric oxide and arterial disease. *J Vasc Surg* 40: 187–193, 2004.
3. **Baumbach GL and Heistad DD.** Cerebral circulation in chronic arterial hypertension. *Hypertension* 12: 89–95, 1988.
4. **Baumgartner HR and Studer A.** Effects of vascular catheterization in normo- and hypercholesteremic rabbits. *Pathol Microbiol (Basel)* 29: 393–405, 1966 (in German).
5. **Bihoreau MT, Gauguier D, Kato N, Hyne G, Lindpaintner K, Rapp JP, James MR, and Lathrop GM.** A linkage map of the rat genome derived from three F_2 crosses. *Genome Res* 7: 434–440, 1997.
6. **Bochaton-Piallat ML, Gabbiani F, Redard M, Desmouliere A, and Gabbiani G.** Apoptosis participates in cellularity regulation during rat aortic intimal thickening. *Am J Pathol* 146: 1059–1064, 1995.
7. **Brown DM, Matise TC, Koike G, Simon JS, Winer ES, Zangen S, McLaughlin MG, Shiozawa M, Atkinson OS, Hudson JR Jr, Chakravarti A, Lander ES, and Jacob HJ.** An integrated genetic linkage map of the laboratory rat. *Mamm Genome* 9: 521–530, 1998.
8. **Bulkley BH and Hutchins GM.** Accelerated "atherosclerosis." A morphologic study of 97 saphenous vein coronary artery bypass grafts. *Circulation* 55: 163–169, 1977.
9. **Cable DG, O'Brien T, Schaff HV, and Pompili VJ.** Recombinant endothelial nitric oxide synthase-transduced human saphenous veins: gene therapy to augment nitric oxide production in bypass conduits. *Circulation* 96: II-173–II-178, 1997.
10. **Cai WJ, Kocsis E, Luo X, Schaper W, and Schaper J.** Expression of endothelial nitric oxide synthase in the vascular wall during arteriogenesis. *Mol Cell Biochem* 264: 193–200, 2004.
11. **Capdeville M, Coutard M, and Osborne-Pellegrin MJ.** Spontaneous rupture of the internal elastic lamina in the rat: the manifestation of a genetically determined factor which may be linked to vascular fragility. *Blood Vessels* 26: 197–212, 1989.
12. **Chen L, Daum G, Chitaley K, Coats SA, Bowen-Pope DF, Eigenthaler M, Thumati NR, Walter U, and Clowes AW.** Vasodilator-stimulated phosphoprotein regulates proliferation and growth inhibition by nitric oxide in vascular smooth muscle cells. *Arterioscler Thromb Vasc Biol* 24: 1403–1408, 2004.
13. **Churchill PC, Churchill MC, Bidani AK, Griffin KA, Picken M, Pravenec M, Kren V, St Lezin E, Wang J-M, Wang N, and Kurtz TW.** Genetic susceptibility to hypertension-induced renal damage in the rat: evidence based on kidney-specific genome transfer. *J Clin Invest* 100: 1373–1380, 1997.
14. **Cicila GT, Choi C, Dene H, Lee SJ, and Rapp JP.** Two blood pressure/cardiac mass quantitative trait loci on chromosome 3 in Dahl rats. *Mamm Genome* 10: 112–116, 1999.
15. **Cicila GT, Garrett MR, Lee SJ, Liu J, Dene H, and Rapp JP.** High-resolution mapping of the blood pressure QTL on chromosome 7 using Dahl rat congenic strains. *Genomics* 72: 51–60, 2001.
16. **Clowes AW, Reidy MA, and Clowes MM.** Mechanisms of stenosis after arterial injury. *Lab Invest* 49: 208–215, 1983.
17. **Crissman RS and Guilford W.** The three-dimensional architecture of the elastic-fiber network in canine hepatic portal system. *Am J Anat* 171: 401–413, 1984.

Downloaded from physiolgenomics.physiology.org on May 21, 2008

18. **deBlois D, Tea BS, Than VD, Tremblay J, and Hamet P.** Smooth muscle apoptosis during vascular regression in spontaneously hypertensive rats. *Hypertension* 29: 340–349, 1997.
19. **Foegh ML, Asotra S, Howell MH, and Ramwell PW.** Estradiol inhibition of arterial neointimal hyperplasia after balloon injury. *J Vasc Surg* 19: 722–726, 1994.
20. **Galis ZS, Johnson C, Godin D, Magid R, Shipley JM, Senior RM, and Ivan E.** Targeted disruption of the matrix metalloproteinase-9 gene impairs smooth muscle cell migration and geometrical arterial remodeling. *Circ Res* 91: 852–859, 2002.
21. **Garrett MR, Dene H, Walder R, Zhang QY, Cicila GT, Assadnia S, Deng AY, and Rapp JP.** Genome scan and congenic strains for blood pressure QTL using Dahl salt-sensitive rats. *Genome Res* 8: 711–723, 1998.
22. **George SJ and Dwivedi A.** MMPs, cadherins, and cell proliferation. *Trends Cardiovasc Med* 14: 100–105, 2004.
23. **Harris EL, Stoll M, Jones GT, Granados MA, Porteous WK, Van Rij AM, and Jacob HJ.** Identification of two susceptibility loci for vascular fragility in the Brown Norway rat. *Physiol Genomics* 6: 183–189, 2001.
24. **Healy DA, Zierler RE, Nicholls SC, Clowes AW, Primozich JF, Bergelin RO, and Strandness DE Jr.** Long-term follow-up and clinical outcome of carotid restenosis. *J Vasc Surg* 10: 662–668, 1989.
25. **Julier C, Delepine M, Keavney B, Terwilliger J, Davis S, Weeks DE, Bui T, Jeunemaitre X, Velho G, Froguel P, Ratcliffe P, Corvol P, Soubrier F, and Lathrop GM.** Genetic susceptibility for human familial essential hypertension in a region of homology with blood pressure linkage on rat chromosome 10. *Hum Mol Genet* 6: 2077–2085, 1997.
26. **Knipp BS, Ailawadi G, Ford JW, Peterson DA, Eagleton MJ, Roelofs KJ, Hannawa KK, Deogracias MP, Ji B, Logsdon C, Graziano KD, Simeone DM, Thompson RW, Henke PK, Stanley JC, and Upchurch GR Jr.** Increased MMP-9 expression and activity by aortic smooth muscle cells after nitric oxide synthase inhibition is associated with increased nuclear factor-κB and activator protein-1 activity. *J Surg Res* 116: 70–80, 2004.
27. **Kuchulakanti P and Waksman R.** Therapeutic potential of oral antiproliferative agents in the prevention of coronary restenosis. *Drugs* 64: 2379–2388, 2004.
28. **Lafont A, Guzman LA, Whitlow PL, Goormastic M, Cornhill JF, and Chisolm GM.** Restenosis after experimental angioplasty: intimal, medial, and adventitial changes associated with constrictive remodeling. *Circ Res* 76: 996–1002, 1995.
29. **Lander ES and Botstein D.** Mapping mendelian factors underlying quantitative traits using RFLP linkage maps. *Genetics* 12: 185–199, 1989.
30. **Lander ES and Kruglyak L.** Genetic dissection of complex traits: guidelines for interpreting and reporting linkage results. *Nat Genet* 11: 241–247, 1995.
31. **Lee WS, Harder JA, Yoshizumi M, Lee ME, and Haber E.** Progesterone inhibits arterial smooth muscle cell proliferation. *Nat Med* 3: 1005–1008, 1997.
32. **Liu MW, Roubin GS, and King SB 3rd.** Restenosis after coronary angioplasty. Potential biologic determinants and role of intimal hyperplasia. *Circulation* 79: 1374–1387, 1989.
33. **Liu Y, Hudetz AG, Knaus HG, Rusch NJ, Baumbach GL, and Heistad DD.** Increased expression of Ca^{2+}-sensitive K^+ channels in the cerebral microcirculation of genetically hypertensive rats: evidence for their protection against cerebral vasospasm. *Circ Res* 82: 729–737, 1998.
34. **Lukashev ME and Werb Z.** ECM signalling: orchestrating cell behaviour and misbehaviour. *Trends Cell Biol* 8: 437–441, 1998.
35. **Manly KF, Cudmore RH Jr, and Meer JM.** Map Manager QTX, cross-platform software for genetic mapping. *Mamm Genome* 12: 930–932, 2001.
36. **Merrilees MJ and Beaumont B.** Structural heterogeneity of the diffuse intimal thickening and correlation with distribution of TGF-β1. *J Vasc Res* 30: 293–302, 1993.
37. **Merrilees MJ, Tiang KM, and Scott L.** Changes in collagen fibril diameters across artery walls including a correlation with glycosaminoglycan content. *Connect Tissue Res* 16: 237–257, 1987.
38. **Moncada S.** Adventures in pharmacology, aspirin, prostacyclin and nitric oxide. *Methods Find Exp Clin Pharmacol* 19, *Suppl* A: 3–5, 1997.
39. **Nathe TJ, Deou J, Walsh B, Bourns B, Clowes AW, and Daum G.** Interleukin-1β inhibits expression of p21(WAF1/CIP1) and p27(KIP1) and enhances proliferation in response to platelet-derived growth factor-BB in smooth muscle cells. *Arterioscler Thromb Vasc Biol* 22: 1293–1298, 2002.
40. **Nikol S, Isner JM, Pickering JG, Kearney M, Leclerc G, and Weir L.** Expression of transforming growth factor-β1 is increased in human vascular restenosis lesions. *J Clin Invest* 90: 1582–1592, 1992.
41. **Orlov SN, Dam TV, Tremblay J, and Hamet P.** Apoptosis in vascular smooth muscle cells: role of cell shrinkage. *Biochem Biophys Res Commun* 221: 708–715, 1996.
42. **Ozaki M, Kawashima S, Yamashita T, Hirase T, Namiki M, Inoue N, Hirata K, Yasui H, Sakurai H, Yoshida Y, Masada M, and Yokoyama M.** Overexpression of endothelial nitric oxide synthase accelerates atherosclerotic lesion formation in apoE-deficient mice. *J Clin Invest* 110: 331–340, 2002.
43. **Paradise NF, Pilati CF, Payne WR, and Finkelstein JA.** Left ventricular function of the isolated, genetically obese rat's heart. *Am J Physiol Heart Circ Physiol* 248: H438–H444, 1985.
44. **Paterson AH, Lander ES, Hewitt JD, Peterson S, Lincoln SE, and Tanksley SD.** Resolution of quantitative traits into Mendelian factors by using a complete linkage map of restriction fragment length polymorphisms. *Nature* 335: 721–726, 1988.
45. **Powell JS, Muller RM, and Baumgartner HR.** Suppression of the vascular response to injury: the role of angiotensin-converting enzyme inhibitors. *J Am Coll Cardiol* 17: 137B–142B, 1991.
46. **Pravenec M, Gauguier D, Schott JJ, Buard J, Kren V, Bila C, Szpirer C, Szpirer J, Wang JM, Huang H, St Lezin E, Spence AM, Flodman P, Printz M, Lathrop GM, Vergnaud G, and Kurtz TW.** Mapping of quantitative trait loci for blood pressure and cardiac mass in the heart by genome scanning of recombinant inbred strains. *J Clin Invest* 96: 1973–1978, 1995.
47. **Rapp JP.** Genetic analysis of inherited hypertension in the rat. *Physiol Rev* 8: 135–172, 2000.
48. **Sarzani R, Brecher P, and Chobanian AV.** Growth factor expression in aorta of normotensive and hypertensive rats. *J Clin Invest* 83: 1404–1408, 1989.
49. **Schork NJ, Krieger JE, Trolliet MR, Franchini KG, Koike G, Krieger EM, Lander ES, Dzau VJ, and Jacob HJ.** A biometrical genome search in rats reveals the multigenic basis of blood pressure variation. *Genome Res* 5: 164–172, 1995.
50. **Stoll M, Kwitek-Black AE, Cowley AW Jr, Harris EL, Harrap SB, Krieger JE, Printz MP, Provoost AP, Sassard J, Jacob HJ, Schork NJ, Krieger JE, Trolliet MR, Franchini KG, Koike G, Krieger EM, Lander ES, Dzau VJ, Jacob HJ, Pravenec M, Gauguier D, Schott JJ, Buard J, Kren V, Bila V, Szpirer C, Szpirer J, Wang JM, and Huang H.** New target regions for human hypertension via comparative genomics. *Genome Res* 10: 473–482, 2000.
51. **Taubman MB, Rollins BJ, Poon M, Marmur J, Green RS, Berk BC, and Nadal-Ginard B.** JE mRNA accumulates rapidly in aortic injury and in platelet-derived growth factor-stimulated vascular smooth muscle cells. *Circ Res* 70: 314–325, 1992.
52. **Von der Leyen HE, Gibbons GH, Morishita R, Lewis NP, Zhang L, Nakajima M, Kaneda Y, Cooke JP, and Dzau VJ.** Gene therapy inhibiting neointimal vascular lesion: in vivo transfer of endothelial cell nitric oxide synthase gene. *Proc Natl Acad Sci USA* 92: 1137–1141, 1995.
53. **Ways JA, Cicila GT, Garrett MR, and Koch LG.** A genome scan for loci associated with aerobic running capacity in rats. *Genomics* 80: 13–20, 2002.
54. **Wilcox JN, Smith KM, Williams LT, Schwartz SM, and Gordon D.** Platelet-derived growth factor mRNA detection in human atherosclerotic plaques by in situ hybridization. *J Clin Invest* 82: 1134–1143, 1988.
55. **Yin FCP, Spurgeon HA, Rakusan K, Weisfeldt ML, and Lakatta EG.** Use of tibial length to quantify cardiac hypertrophy: application in the aging rat. *Am J Physiol Heart Circ Physiol* 243: H941–H947, 1982.
56. **Zimdahl H, Kreitler T, Gosele C, Ganten D, and Hubner N.** Conserved synteny in rat and mouse for a blood pressure QTL on human chromosome 17. *Hypertension* 39: 1050–1052, 2002.

Downloaded from physiolgenomics.physiology.org on May 21, 2008